Miner Petrol (2017) 111:399–416
DOI 10.1007/s00710-016-0477-8

ORIGINAL PAPER

Stable isotope (C, O, H) characteristics and genesis of the Tazheran brucite marbles and skarns, Olkhon region, Russia

Anna Doroshkevich[1,2] · **Eugene Sklyarov**[3,4] · **Anastasia Starikova**[1,5] · **Vladimir Vasiliev**[2] · **German Ripp**[2] · **Ivan Izbrodin**[2] · **Viktor Posokhov**[2]

Received: 20 October 2015 / Accepted: 28 September 2016 / Published online: 7 October 2016

Abstract Stable isotope compositions are examined for brucite marble and Mg-skarn that occur in the southern part of the Tazheran massif, Olkhon region, Russia. Brucite marble exhibits a narrow range in $\delta^{18}O$ of +23.3 to +26.2 ‰ and shows carbon isotope depletion of −1.9 to −4.4 ‰) as compared with the country dolomite isotope compositions (+2.0 to +2.4 ‰) which is explained by both decarbonation processes and participation of fluids depleted in ^{13}C. The emplacement of brucite marble was accompanied by the formation of endo- and exoskarn at the contact between syenite and brucite marble. $\delta^{18}O$ profiles across the contact show a typical decrease towards the syenite side interpreted as the result of fluid/rock interaction and influx of magmatic fluids. Finally, we discuss the mechanisms of brucite marble emplacement and consider three possible ways of producing these rocks: (1) injection of dolomite with subsequent transformation to periclase marble and then to brucite marble; (2) injection of periclase marble with a following replacement of periclase by brucite or injection of brucite marble; (3) crustal water-rich carbonate melt. We favor models 2 and 3 and discuss their strengths and weaknesses.

Keywords Brucite marble · Skarn · Tazheran gabbro-syenite massif · Olkhon collision system · Stable isotopes · Fluid-rock interaction · Decarbonation · Fluid depleted in C^{13}

Editorial handling: C. Hauzenberger

✉ Anna Doroshkevich
doroshkevich@igm.nsc.ru

[1] Sobolev Institute of Geology and Mineralogy Siberian Branch Russian Academy of Sciences, Novosibirskpr. Akademika Koptyuga, 3, 630090, Russia

[2] Geological Institute SB RAS, Ulan-UdeSakhyanovoy Str., 6a, 670047, Russia

[3] Institute of the Earth's Crust SB RAS, IrkutskLermontova Str., 128, 664033, Russia

[4] Far Eastern Federal University, Vladivostok8 Sukhanov Street, 690950, Russia

[5] Novosibirsk State University, NovosibirskPirogova Str., 1, 630090, Russia

Introduction

The Tazheran massif and/or Tazheran skarn has been well known to mineralogists from the beginning of the latter half of the 20th century. New minerals were discovered here, such as tazheranite ($(Zr,Ti,Ca)O_2$; Konev et al. 1969) and azoproite ($(Mg,Fe^{2+})_2(Fe^{3+},Ti,Mg)(BO_3)O_2$; Konev et al. 1970). Rare minerals and unusual compositions of known mineral groups, such as melilite, magnesian kirschteinite were also found and the occurrences were cited in leading mineralogical handbooks (e.g., Deer et al. 1997). Perovskite from the Tazheran massif is especially important because it is used as a standard for dating by secondary ion mass spectrometric (SHRIMP) method in several laboratories worldwide (Ireland et al. 1990; Kinni et al. 1997; Yang et al. 2009; Li et al. 2010). At the same time, there is practically no geological and mineralogical information in recent papers about the Tazheran massif. Konev and Samoylov (1974) described in detail the Tazheran massif, but this book is not translated into English and therefore is poorly known to the international geological community outside Russia. From the above mentioned references one may get an impression that the Tazheran was formed by classical skarn processes at the contact of a syenite intrusion with carbonate rocks (e.g., Povoden et al. 2002; Gallien et al. 2007): zonation of skarn reflects the geometry of the pluton contact and fluid flow; skarn is zoned

from endoskarn throughout exoskarn to pyroxene-rich zone and the skarn front. The authors of the first description of the massif (Konev and Samoylov 1974) attempted to fit available facts into the classical model of skarn formation despite some inconsistencies with the model. First of all, any signs of interaction between syenite and country calcite marble are absent at the contacts of the massif and observed only at the contact of brucite marble bodies within the massif. Konev and Samoylov (1974) interpreted the latter as xenoliths in syenites. Secondly, brucite marbles which is usually described as hydration product of periclase marble formed during contact metamorphism of dolomite, is represented by bodies of complex shape and various sizes in syenites as well as veins cross-cutting gabbro and syenites (Sklyarov et al. 2009, 2013). In addition, dolomite is absent in the frame of the Tazheran massif although the rock is common in other areas of the Olkhon collision system. It is very important that in contrast to the classical model of skarn formation at static (stable) conditions, syenite and other magmatic rocks were emplaced during active strike-slip tectonics during the formation of the Early Paleozoic collision belt (Fedorovsky et al. 2010). It caused a syn-deformational intrusion of multiple pulses of syenite and mafic magmas. The list of inconsistencies with the classical model of skarn formation will be continued below, but the above-mentioned facts are already enough to seriously challenge the validity of the model proposed by Konev and Samoylov (1974). Searching for alternatives, Sklyarov et al. (2013) proposed crustal carbonate melting as a model for the formation of calc-silicate and brucite marble of the massif that intruded simultaneously with nepheline syenite and subalkaline gabbro. In this study, we present the first stable isotope (C, O, H) data on brucite marble and rocks from the skarn zone of the massif to test the "classic" skarn and crustal carbonate melting models. On the basis of these new data, we show that brucite marble cannot be a product of fluid-rock interaction in the course of contact metamorphism during emplacement of the Tazheran magmatic rocks and suggest the most appropriate scenario of C and O isotope depletion of brucite marble. Finally, we discuss the presumable mechanisms of brucite marble emplacement.

Geological background

The massif with an area of 6 km^2 is situated on the shore of Lake Baikal (Figs. 1 and 2), and is exposed pretty well. The massif is positioned at the center of a large shear loop that is part of a complex structure of metamorphic rocks of the Olkhon collision system in the Western Baikal region (Figs. 1 and 2). The system is situated on the eastern flank of the Early Paleozoic accretion-collision belt along the southern border of the Siberian craton (Dobretsov and Buslov 2007) and is comprised of various magmatic and metamorphic rocks. Two main zones (terranes) of the system have been distinguished (Fedorovsky et al. 1995; Fedorovsky 2004): The Anga zone, regarded as a fragment of a Cambrian island arc (Gladkochub et al. 2014; Donskaya et al. in press), is composed mostly of amphibolite, marble and gabbro massifs, and minor granite and gneiss (Fig. 1). The Olkhon zone, being a complex collage of cratonic, back arc basin and ophiolite fragments, comprising gneiss, marble, amphibolite, quartzite, granite, minor mafic and ultramafic massifs. The metamorphic grade corresponds to amphibolite facies (550–650 °C) for a large part of the Olkhon collision system and it reaches granulite facies in a zone adjacent to the collision suture, separating it from the Siberian craton. The system has been formed in a time span between 500 to 460 Ma by several stages of tectonic events which were accompanied by metamorphic and magmatic processes, as a result of oblique collision of terranes of the Paleoasian ocean to the Siberian craton (Donskaya et al. in press). Age and nature of protholiths of

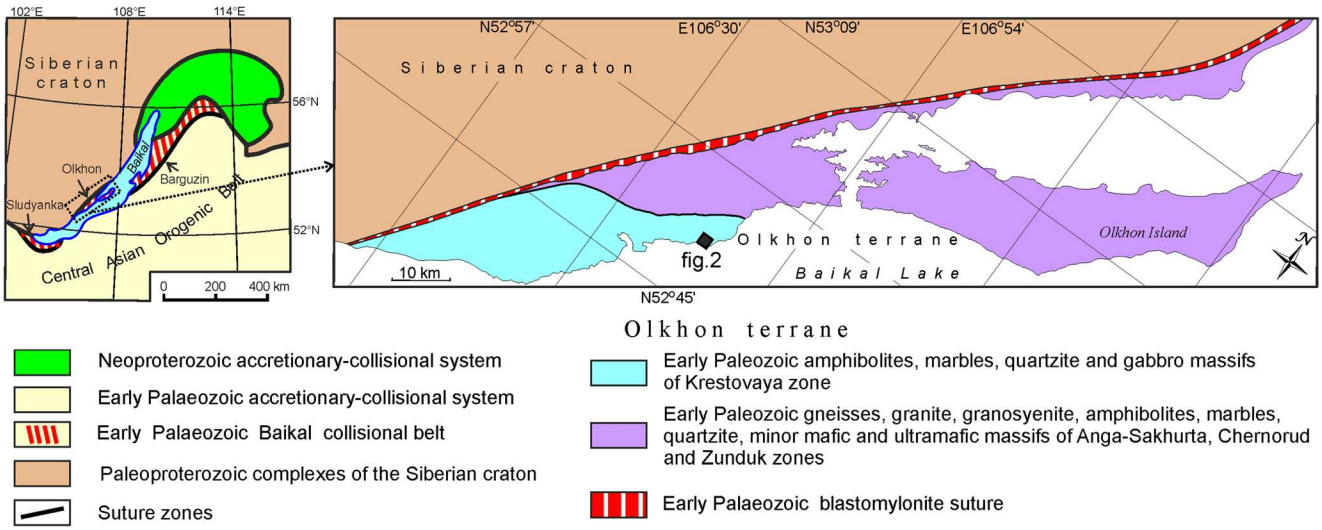

Fig. 1 Scheme of the Olkhon collision system in the Western Baikal region (after Donskaya et al. in press)

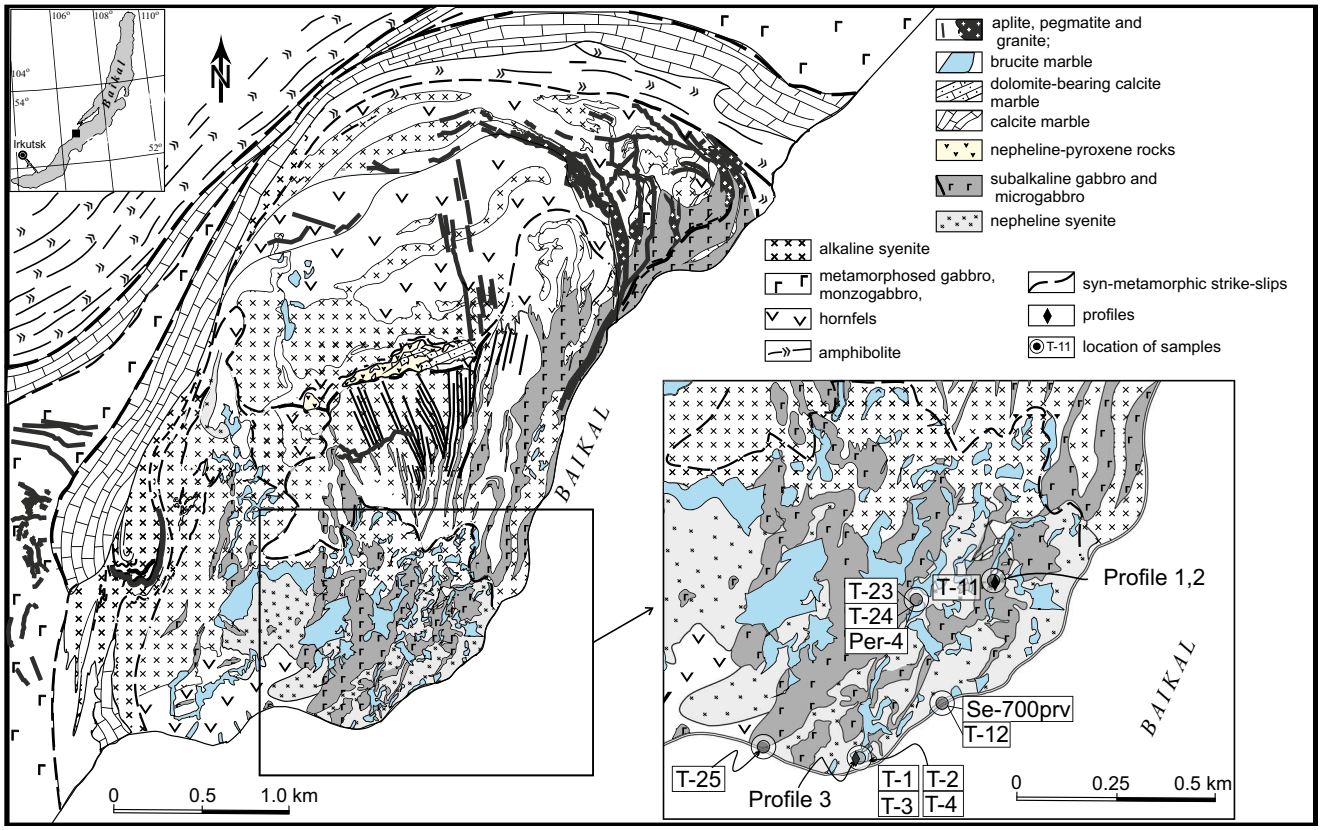

Fig. 2 Simplified geological map of the Tazheran complex (modified after Fedorovsky et al. 2010) with location of samples

the metamorphic rocks are quite debatable; available isotopic data (Donskaya et al. in press) show a wide range from 2000 to 460 Ma. High abundance of graphite (up to 20 %) in various kinds of rocks (marble, gneiss, pegmatite, quartzite and amphibolite) is noteworthy.

The geology of the Tazheran massif and detailed petrographic descriptions of the major rock types have been presented in a number of publications (e.g., Konev et al. 1967; Konev and Samoylov 1974; Fedorovsky et al. 2009, 2010; Sklyarov et al. 2009, 2013; Starikova et al. 2014). We use the traditional term "Tazheran massif" but actually it is a complex structure composed of a large variety of rocks (Fig. 2). Alkaline syenite is the most widespread rock type (Fig. 2) which appears as massive, medium- to coarse-grained rock in the central part of the massif, and as foliated type at the marginal parts. The main rock-forming minerals in the rock are alkali-feldspar and clinopyroxene. Minor and accessory minerals are amphibole, biotite, magnetite, titanite, apatite, calcite and zircon. The feldspar is microcline with $Or_{57-60}Ab_{40-62}An_{0-3}$composition. Clinopyroxene is augite and aegirine-augite. It is usually replaced by hastingsite and/or biotite. Nepheline syenite is exposed in the southern and eastern parts of the massif. They typically form vein-like and irregular bodies from one meter up to 100–150 m thickness. Petrographic description and mineral chemistry of the rocks are given in "Conclusions" section. Subalkaline gabbro forms dykes of up to 3–7 m thickness in the center of the massif and bodies of elongated bizarre shape within brucite marble. Most commonly gabbro is strongly altered and composed of hornblende, biotite and plagioclase, sometimes with relics of augite. Minor minerals are magnetite, apatite and titanite. Plagioclase is anorthite-rich (An_{57-68}), mol % orthoclase content is generally low. Veins of pegmatite, aplite and granite are the latest magmatic rocks in the massif.

Beerbachite (epidiorite) occurs mainly in the northern part of the massif. The rock is fine-grained with a massive texture and granular structure. It is composed of orthopyroxene, clinopyroxene, pargasite and plagioclase sometimes with minor olivine, spinel and biotite. In areas of the most intense late metamorphic overprint the rocks show metamorphic banding and have a significantly higher amphibole mode. Sometimes the beerbachite contains relics of dolerite.

Country dolomite marble occurs at a significant distance from the massif (about 12 km) while calcite marble has tectonic contacts with the rocks of the massif (Fig. 2). Brucite marble occurs in the southern part of the massif (Fig. 2). There are some important features of the rock distribution:

1) brucite marble occurs only within the massif being absent at the frame of the massif (Fig. 2). There are also no dolomite marble around the massif;

2) along with relatively large blocks (up to300x100 m size) the brucite marble forms bodies of various shape in a complex "mixture" of syenite, gabbro and marble (Fig. 2) including veins (up to 3 m thick) crosscutting syenite and gabbro (Fig. 3). Moreover, apophyses of brucite marble within syenite have also been documented;
3) syenite is often foliated as a result of post-crystallization ductile deformations, and in several places, where the contact between syenite and brucite marble is well exposed, foliation is almost perpendicular to the contact;
4) series of thin parallel veins of forsterite calc-silicate rocks (0.5-3 cm thick) usually occur at the brucite marble oriented parallel to the contacts to nepheline syenite (see Fig. 3c);
5) brucite marble sometimes contains rounded globules of nepheline syenite ranging in size from 0.5x1 to 100x100 m (Fig. 3c). The syenite has a magmatic texture and does not display any sign of shear in marginal parts of the globules. Instead, envelopes of zebra rocks (5–30 cm in thickness) are usual (see below).

Dolomite-bearing calcite marble is located in the center of the massif (Fig. 2) between alkaline syenite and hornfels.

An important feature of the massif is the presence of a wide range of metasomatic rocks (Konev and Samoylov 1974; Starikova et al. 2014) formed at the contact between brucite marble and nepheline syenite, as well as separate individual bodies. Most of the metasomatic occurrences are too small and cannot be displayed on a geological map except nepheline-pyroxene rocks associated with dolomite-bearing calcite marble in the central part of the massif (Fig. 2). There are three types of metasomatic rocks spatially separated in the area of the massif (Starikova et al. 2014): alkaline metasomatic rocks, Mg-skarns and Ca-skarns.

Ca-skarns occur within calcite marble and consists of garnet, pyroxene, amphibole and zoisite. Nepheline-pyroxene alkaline metasomatic rocks are mapped in the central part of the massif at contacts between dolomite-bearing calcite marble and beerbachite. The rocks also form angular fragments of various sizes (from several centimeters to tens of meters) in

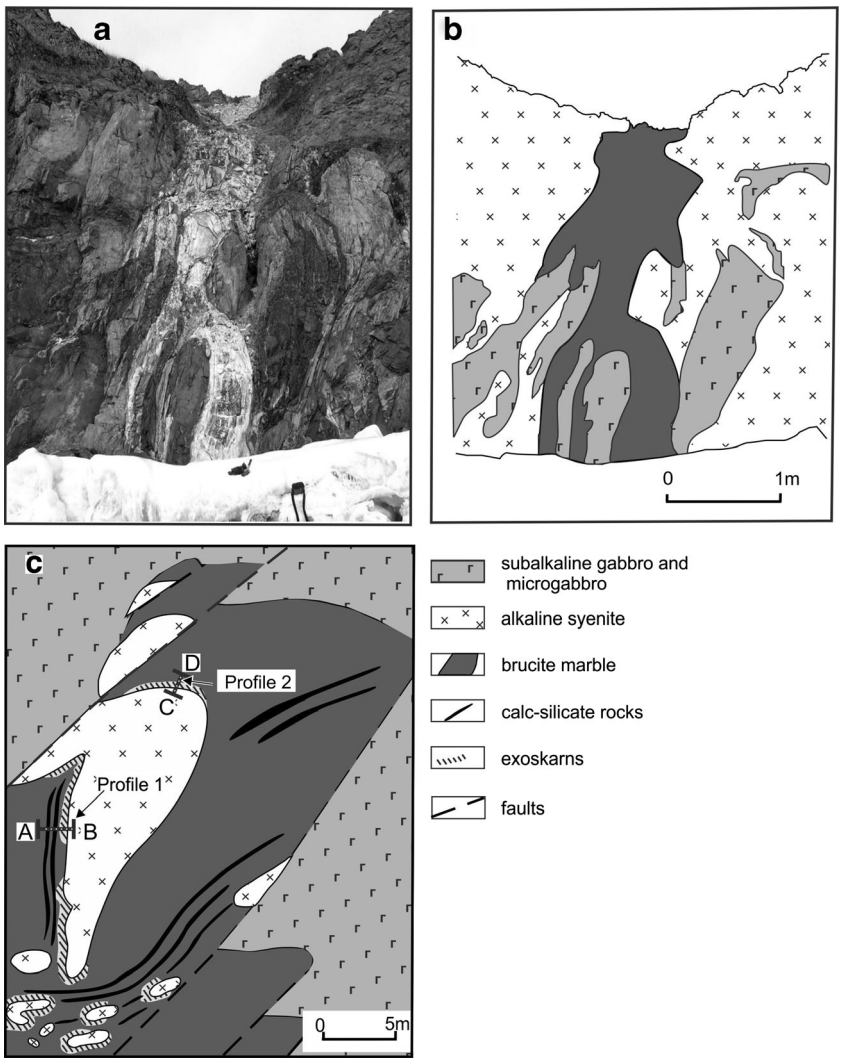

Fig. 3 Schematic maps of the selected brucite marble bodies (after Sklyarov et al. 2013): **a**, **b** – Photograph and sketch after a photograph of a vein-like body of brucite marble cross-cutting syenite and gabbro. **c** – detail of the skarn rocks and brucite marble distribution and their relationship to magmatic rocks. The position of profiles with samples collected as part of this study are shown

marbles. The origin of Ca-skarns and alkaline metasomatic rocks is a special problem outside the scope of this study.

Magnesian metasomatic rocks occur in the southern part of the massif as a reaction zone (usually centimeters to decimeters, rarely meters thick) between nepheline syenite and brucite marble and as veins of calc-silicate rocks in marbles, syenites and gabbro. A generalized geological profile across the skarn zone comprises nepheline syenite → endoskarn (calcite-bearing nepheline-clinopyroxene zone or rarely calcite-bearing spinel-clinopyroxene zone) → exoskarn (zebra rocks consisting of millimeter- to centimeter-scale interleaved bands of mafic minerals and bands of calcite (reaching 1 m width)) → brucite marble with forsterite-calcite veinlets oriented parallel to contacts (<1–2 cm thick). Clinohumite, brucite and apatite are rare minerals in the forsterite-calcite veins. Another type of calc-silicate rocks forms veins that occur within brucite marble but also in other types of rocks within the massif (alkaline syenite and gabbro). They show varying thickness from 5 cm to 2 m and have a complex shape. The rocks are composed of calcite, forsterite, spinel, with accessory calzirtite, tazheranite, perovskite and others.

Magmatic and metasomatic rocks of the massif are well dated by the U–Pb method on zircon, tazheranite and baddeleyite (Sklyarov et al. 2009; Starikova et al. 2014) and the age falls in the interval of 460–470 Ma. The alkaline syenite and beerbachite are the oldest (470 Ma), while nepheline syenite, subalkaline gabbro and calc-silicate veins intruded at a time interval between 465 to 455 Ma.

Two important points should be emphasized: (1) Contacts of the composite massif are tectonic; there are no traces of interaction between magmatic rocks of the massif and embedding calcite marble and metagabbro. The massif's emplacement was syn-tectonic (syn-metamorphic). (2) The metasomatic rocks occur inside of the massif as narrow zones between brucite marble and nepheline syenite or as veins cross-cutting brucite marble, alkaline syenite and gabbro.

Analytical methods

The sampling locations are shown in Fig. 2. Four profiles approximately perpendicular to the contact between brucite marble, syenite and gabbro were sampled (Fig. 3). The approximate distances of the samples from the contact with magmatic rocks are listed in Table 1.

Energy-dispersive X-ray spectrometry in combination with backscattered electrons (BSE) imaging was used for textural studies and selection of areas for quantitative microprobe analysis. Mineral compositions were determined using a JEOL JXA-8100 electron probe micro-analyser (EPMA) operated in wave length-dispersion mode at the. For silicate minerals, a beam current of 30 nA and an acceleration voltage of 15 kV were used; for Fe-Ti oxides current and voltage were set to 20 nA and 20 kV, respectively. Peak counting times were 16 s for major elements and 30–60 s for minor elements. For calibration, both natural minerals and synthetic phases were used. Brucite samples have been studied by means of a JobinYvon LabRAM HR800 Raman spectrometer.

Carbonates were analyzed for oxygen and carbon isotopes, and $\delta^{13}C$, $\delta^{18}O$ and δD values were acquired using a Finnigan MAT 252 and 253 sensitive mass spectrometers. CO_2 was extracted from calcite at 60 °C during 2–4 h with phosphoric acid. Aliquots of CO_2 were sampled automatically and introduced to the mass spectrometer in a continuous He flow. NBS-18 and NBS-19 international reference materials were used to assess the accuracy of the mass spectrometer. The analytical errors for the $\delta^{18}O$ and $\delta^{13}C$ determination were ±0.05 ‰ or less and ± 0.1 ‰, accordingly.

Analyses of graphite were carried out using an elemental analyzer (Thermo Flash EA 1112) combined with stable isotope ratio mass spectrometer. The system was calibrated using NBS-18 and NBS-19 as a reference material. The precision of the analysis is close to 0.3 ‰.

Oxygen-isotope analyses for silicates and oxides were made using the laser fluorination method of Sharp (1990). Samples were heated with a 100 W CO_2 laser in a BrF_5 atm. NBS-28 (quartz) and NBS-30 (biotite) were used as reference materials for $\delta^{18}O$ analysis. Garnet UWG-2 was used as secondary reference; this material was analyzed during each run to ensure accuracy. Based on these data and the reproducibility of duplicate measurements, the $\delta^{18}O$ values of unknowns are accurate to within 0.2 ‰.

Hydrogen isotope compositions were determined with a high temperature conversion elemental analyzer (TC/EA) using a method adapted after that by Sharp et al. (2001). The raw data for δD values were normalized using NBS-30 biotite. The δD isotope compositions of the laboratory standards measured in this study are reproducible to within ±2 ‰.

The process of Rayleigh volatilization for open system was calculated using Eq. (1) (Valley 1986) and the values of isotope fractionation according to Chacko et al. (1991).

$$\delta_f - \delta_i = 1000\left(F^{(\alpha-1)} - 1\right) \quad (1)$$

where δ_i and δ_f are the initial and final isotope values of the rock, α is the fractionation factor and F is the mole fraction of relevant element (C or O) in the residual rock.

Effect of fluid-rock interaction in closed system (multipass model) was evaluated by the Eqs. (2) and (3) (Taylor 1977) and the values of isotope fractionation according to Zheng (1999) ($\alpha_{Cal\text{-}H2O}$) and Chacko et al. (1991) ($\alpha_{Cal\text{-}CO2}$).

$$F/R = \left(\delta^{18}O^{f}_{r} - \delta^{18}O^{i}_{r}\right) / \left(\delta^{18}O^{i}_{fl} - \delta^{18}O^{f}_{r} + \Delta\right) \quad (2)$$

$$X_{CO2}\,F/R = \left(\delta^{13}C^{f}_{r} - \delta^{13}C^{i}_{r}\right) / \left(\delta^{13}C^{i}_{fl} - \delta^{13}C^{f}_{r} + \Delta\right) \quad (3)$$

Table 1 Values $\delta^{18}O$ and $\delta^{13}C$ for carbonates from rocks of skarn zone and country rocks, Tazheran massif

Sample		Rock types	Distance from igneous contact (cm)	$\delta^{13}C_{(VPDB)}$	$\delta^{18}O_{(VSMOW)}$
Profile 1 AB	1-1	Endoskarn	5	−3.1	16.2
	1-2	Exoskarn ("zebra" rocks)	11	−2.9	21.2
	1-3	Exoskarn. contact with brucite marble	21	−3.00	23.9
	1-4	Brucite marble	31	−3.4	23.00
	1-5		69	−3.40	23.90
	1-6	Calc-silicate rock	83	−3.7	24.5
	1-7	Brucite marble	87	−3.5	23.5
	1-9		90	−3.3	23.3
	1-10	Calc-silicate rock	100	−2.9	23.9
	1-11	Brucite marble	215	−3.4	25.2
Profile 2 CD	2-1	Endoskarn	3	−3.1	17.1
	2-2	Exoskarn ("zebra" rocks)	5	−2.6	17.8
	2-3	Exoskarn. contact with brucite marble	10	−2.8	22.1
	2-4	Brucite marble	38	−3.3	23.3
	2-5		85	−1.9	26.2
Profile 3 AB	3-1	Vein-like body of brucite marble, contact with gabbro	6	−3.5	20
	3-2	Vein-like body of brucite marble, proximal zone	21	−2.4	25.8
	3-3	Vein-like body of brucite marble, contact with gabbro	2	−3.3	16.5
Profile 3 CD	3-1a	Vein-like body of brucite marble, contact with gabbro	1	−4.4	14.3
	3-1б	Vein-like body of brucite marble, proximal zone	10	−4.2	17
T12		Endoskarn	4	−3.61	13.63
T12a			3	−3.80	12.80
T2		Exoskarn	9	−2.20	21.76
T11a			7	−3.09	20.19
T11a1			6	−3.10	20.20
Per4		Calc-silicate rock		−3.68	21.74
T4				−3.33	22.97
T-24				−2.50	22.40
Se700prv				−2.30	19.30
T1		Brucite marble	60	−3.48	23.82
T11b			125	−3.35	25.35
T11c1			127	−3.40	25.30
T-25			70	−3.70	24.10
T-23			105	−2.90	26.00
T13		Country calcite marble	7650 (m)	−0.25	24.22
T13a			7600 (m)	−0.60	23.70
5			1000 (m)	0.00	21.10
6			2250 (m)	−2.30	23.10
7			3750 (m)	−2.70	17.80
T14		Dolomite marble	11,700 (m)	2.27	27.48
T14a			12,000 (m)	2.40	27.50

where δ^{f}_{r} and δ^{i}_{r}–final and initial isotope values of the rocks, δ^{f}_{fl} and δ^{i}_{fl}–final and initial isotope values of the fluid, F and R – atomic ratios of elements (C or O) for fluid and rock, Δ - difference in δ values between rock and fluid, X_{CO2} – the mole fraction of carbon in the fluid.

The $\delta^{13}C$-$\delta^{18}O$ trends in an open system (one pass model) were calculated using the Eq. (4) (Taylor 1977).

$$F/R = \ln\left(F/Rc + 1\right) \quad (4)$$

where F/Rc is the value obtained from the close system.

Table 2 EPMAof clinopyroxene and nepheline from rocks of skarn zone, Tazheran massif

Mineral	Nepheline						Clinopyroxene					
Rock type	Nepheline syenite		Transition zone		Endoskarn		Nepheline syenite		Transition zone		Endoskarn	
Oxide(wt. %)												
SiO_2	45.51	45.87	43.54	44.07	44.19	42.47	51.29	49.00	55.39	55.36	53.39	54.66
TiO_2	–	–	–	–	–	–	0.61	1.23	0.17	0.37	0.05	0.06
Al_2O_3	32.64	32.80	33.31	33.13	32.96	34.50	2.05	2.14	1.51	1.87	1.94	1.63
FeO_{tot}	0.10	0.11	0.23	0.21	0.30	0.18	15.48	19.68	4.96	5.21	7.00	1.81
MgO	–	–	–	–	–	–	8.00	4.96	14.42	14.12	13.65	17.06
MnO	–	–	–	–	–	–	0.53	0.91	–	–	–	–
CaO	0.75	0.57	0.07	0.07	0.30	0.15	18.12	20.37	22.00	21.31	23.59	24.67
Na_2O	15.72	15.82	16.22	15.90	16.30	17.18	3.56	1.75	1.81	2.31	0.64	0.34
K_2O	4.54	4.71	6.07	5.76	4.93	5.77	–	–	–	–	–	–
Total	99.26	99.88	99.44	99.13	99.01	100.29	99.64	100.04	100.27	100.56	100.27	100.25
Formulae based on 8 (6) oxygens for nepheline (clinopyroxene)												
Si	1.085	1.087	1.050	1.061	1.063	1.019	1.939	1.916	2.013	2.003	1.969	1.975
Ti	–	–	–	–	–	–	0.017	0.036	−5	0.010	−1	−2
Al	0.917	0.916	0.947	0.940	0.934	0.976	0.091	0.098	0.064	0.080	0.094	0.069
Fe^{+3}	−2	−2	−4	−4	−5	0.003	0.257	0.130	0.029	0.056	0.021	0.001
Fe^{+2}	–	–	–	–	–	–	0.232	0.513	0.122	0.101	0.194	0.053
Mg	–	–	–	–	–	–	0.451	0.289	0.781	0.761	0.750	0.919
Mn	–	–	–	–	–	–	0.017	0.030	–	–	–	–
Ca	0.019	0.015	0.002	0.002	0.008	0.004	0.735	0.854	0.858	0.827	0.933	0.956
Na	0.727	0.727	0.758	0.742	0.760	0.799	0.262	0.133	0.127	0.162	0.046	0.024
K	0.138	0.142	0.187	0.177	0.151	0.177	–	–	–	–	–	–

Here and below: FeO_{tot} = total iron; − = below detection limit estimated as 0.01 wt.%

The process of Rayleigh isotope fractionation during formation of graphite was calculated using Eq. (5) (Ray 2009) and $\alpha_{g\text{-}CO2}$ and $\alpha_{CH4\text{-}CO2}$ values are from Scheele and Hoefs (1992) and Horita (2001), respectively.

$$\delta^{13}\mathrm{Cg} = 10^3\left(\alpha_{g-1}\Big/\left(a-b\Big/f\right)-1\right) + \left(\alpha_{g-1}\Big/\left(a-b\Big/f\right)\right)\delta^{13}\mathrm{Cs} \quad (5)$$

where $\alpha_{g\text{-}1}$ is the fractionation factor of carbon between graphite and the largest source component (CO_2 or CH_4),f is the fraction of remaining carbon in the source (the Eq. 6), a and b parameters are from Eqs. (7) and (8), $r_{CH4\text{-}CO2}$ is the initial molar ratio of CH_4 and CO_2 in the fluid.

$$f = (1-r_{CH4\text{–}CO2})\Big/(1+r_{CH4\text{–}CO2}) \quad (6)$$

$$a = (1+\alpha_{CH4\text{–}CO2})\Big/2 \quad (7)$$

$$b = ((1-r_{CH4\text{–}CO2})(\alpha_{CH4\text{–}CO2}-1))\Big/2(1+r_{CH4\text{–}CO2}) \quad (8)$$

The method of the thermodynamic modelling of phase equilibria (Vasiliev et al. 2009), which has been well tested (Vasiliev et al. 2009; Vasiliev and Damdinov 2013), was applied using the Gibbs free energy minimization "SELEKTOR" code (Karpov et al. 1997). The minimization algorithm implements the modified interior point technique (the IPM-2 algorithm, Chudnenko 2010). A set of potentially possible dependent components have been formed from the databases of thermodynamic properties of gas, solid, and aqueous species (Johnson et al. 1992; SLOP98).

Results

Petrography and mineral chemistry

Below we describe the rocks from contact zones that include nepheline syenite, endo- and exoskarn, calc-silicate rocks and brucite marble as well as country dolomite marble (located at significant distance from the massif) that we use in our constructions. The representative compositions of the main minerals (nepheline, clinopyroxene, spinel, olivine, calcite) are shown in Tables 2, 3, and 4.

Table 3 EMPA of olivine and spinel from rocks of skarn zone, Tazheran massif

Mineral	Spinel				Forsterite					
Rock type	Exoskarn		Calc-silicate rock		Exoskarn		Calc-silicate rock		Forsterite-calcite veinlet	
Oxide(wt. %)										
SiO_2	–	–	–	–	41.16	41.19	41.91	41.84	42.49	42.64
TiO_2	–	–	0.72	0.37	–	–	–	–	–	–
Al_2O_3	66.67	66.16	68.40	69.64	–	–	–	–	–	–
FeO_{tot}	11.01	11.28	3.47	3.24	8.06	8.88	1.02	0.99	–	–
MgO	21.90	22.26	27.40	26.86	50.84	50.35	56.82	57.22	57.24	57.22
MnO	0.28	–	0.04	0.03	0.30	0.40	0.06	0.05	–	–
CaO	–	–	–	–	–	–	0.06	0.10	–	–
Total	100.11	100.02	100.03	100.15	100.36	100.82	99.90	100.22	99.73	99.86
Formulae based on 4 oxygens										
Si	–	–	–	–	0.997	0.997	0.989	0.985	0.998	1.000
Ti	–	–	0.012	0.007	–	–	–	–	–	–
Al	1.954	1.940	1.936	1.965	–	–	–	–	–	–
Fe^{+3}	0.046	0.060	0.037	0.021	–	–	–	–	–	–
Fe^{+2*}	0.183	0.175	0.032	0.043	0.163	0.180	0.020	0.019	–	–
Mg	0.811	0.825	0.980	0.958	1.836	1.817	1.998	2.007	2.004	2.000
Mn	0.006	–	0.001	0.001	0.006	0.008	0.001	0.001	–	–
Ca	–	–	–	–	–	–	0.001	0.003	–	–

Fe_{tot} for forsterite

Nepheline syenite

The rock is medium-grained with trachytoid textures. Nepheline syenite is composed of euhedral nepheline, alkali feldspar crystals, anhedral clinopyroxene grains. Albite and biotite are minor minerals. Apatite, titanite, zircon and magnetite are accessories. Nepheline usually contains solid inclusions of clinopyroxene, rarely biotite and alkali feldspar. Mineral composition is $Ne_{74-77}Ks_{14-15}Qtz_{8-9}$. The CaO content is low (0.4 – 0.8 wt.%). Alkali feldspar shows variations in orthoclase component (74–94 %), with FeO_{tot} and Na_2O concentrations ranging up to 1.0 and 4.5 wt.%, respectively. Clinopyroxene compositions show varying amounts of diopside (Di, 29–46 mol%), hedenbergite (Hed, 23–51 mol%) and aegirine (Aeg, 13–27 mol%) components. A transition zone between endoskarn and nepheline syenite is characterized by increased alkali feldspar and decreased clinopyroxene contents. Titanite, calcite and baddeleyite are accessory minerals here. Clinopyroxene is more Di-rich (73–76 mol%), Hed- and Aeg-poor (9–11 and 3–10 mol%, accordingly) compared with the compositions in nepheline syenite. Nepheline contains less Qtz- (up to 6 %) and more Ks- (up to 19 %) components and has lower concentration of CaO (<0.06 wt.%) than the mineral from nepheline syenite. Calcite forms anhedral grains and has low FeO and MgO contents of up to 0.2 and 0.1 wt.%, accordingly. In some cases, this type of mineralogy is common for late stage alteration of nepheline syenite (Chakrabarty et al. 2016).

Endoskarn forms a narrow zone up to several cm in width. It is massive and is composed of alkali feldspar, clinopyroxene and calcite. Thin (up to 1–2 mm) coronas of clinopyroxene-nepheline symplectitic intergrowths are developed between endoskarn and nepheline syenite (Fig. 4a). Clinopyroxene composition is dominated by diopside (Di, 76–93 mol%), with varying amount of hedenbergite (Hed, 2–19 mol %) and low amount of aegirine (Aeg, up to 3 mol%) components.

Table 4 EMPA (wt. %) of calcite from rocks of skarn zone, Tazheran massif

Rock type	Transition zone		Endoskarn		Exoskarn		Calc-silicate rock		Brucite marble		Forsterite-calcite veinlet	
FeO	0.23	0.20	0.11	0.06	–	–	0.04	0.03	–	–	–	–
MgO	0.07	0.07	0.24	0.10	1.24	1.48	1.21	0.87	3.72	1.88	1.90	1.74
CaO	56.78	58.60	57.29	56.76	50.78	52.71	53.63	53.92	49.24	51.68	51.70	51.09
Total	57.18	58.88	57.70	56.94	52.02	54.19	54.90	54.83	52.96	53.56	53.60	52.83

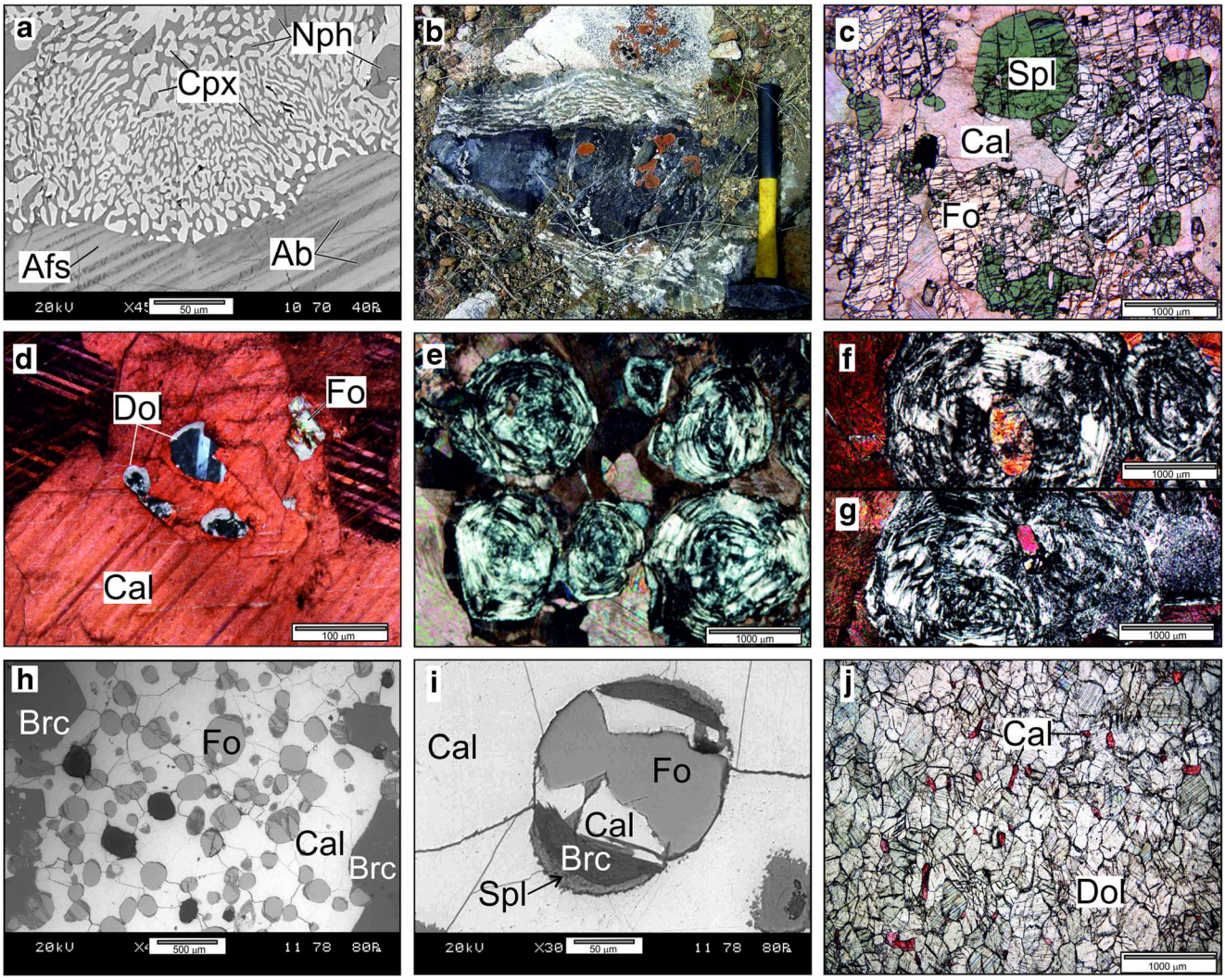

Fig. 4 Photographs and BSE images of: **a** – clinopyroxene-nepheline symplectic intergrowth in transition zone between nepheline syenite and endoskarn; **b** – "zebra" rocks; **c** – distribution of minerals in calc-silicate rocks, **d** – dolomite inclusions in calcite from brucite marbles; **e** – onion-skin oval-shaped grains of brucite in marble; **f** – forsterite, **g** - calcite and clinohumite inclusions in brucite; **h** – forsterite-calcite veinlet in brucite marble; **i** - forsterite surrounded by a corona of brucite-calcite and partially replaced by minerals of serpentine group; **j** – distribution of calcite in country dolomite marbles. Calcite is dyed by alizarine on the **d**, **f**, **g** and **j** photographs. Cpx – clinopyroxene, Nph – nepheline, Ab-albite, Afs – potash feldspar, Cal – calcite, Fo – forsterite, Spl – spinel, Dol – dolomite, Brc – brucite, Srp - minerals of serpentine group

Nepheline is $Ne_{78\text{-}80}Ks_{15\text{-}19}Qtz_{1\text{–}6}$ with low concentrations of CaO (0.08–0.3 wt.%). Calcite composition is similar to the mineral found in nepheline syenites (up to 0.1 wt.% FeO and 0.3 wt.% MgO).

Exoskarn (Zebra rock)

The rock displays a series of dark-colored bands containing up to 90 % fine-grained assemblages of olivine and spinel that alternate with bands composed essentially of relatively coarse-grained calcite (Fig. 4b). These bands range from a few mm to a few cm in width. Fe-Ti oxides, perovskite, baddeleyite, tazheranite, zirconolite, calcirtite are accessory minerals. Calcite contains measurable amounts of MgO (up to 1.5 wt.%). Spinel forms dull green, euhedral to sub-rounded crystals. The mineral contains traces of MnO (up to 0.5 wt.%) and high FeO content (10.5–13 wt.%). TiO_2 is below the detection limit. Olivine is more anhedral as compared to spinel, but it also forms crystals in the calcite groundmass. Sometimes minerals of the serpentine group replace olivine along microcracks and rims. Olivine composition is $Fo_{91\text{–}92}$. The mineral has MnO contents of up to 0.65 wt.%.

Calc-silicate rock

The main rock-forming minerals in calc-silicate rocks are spinel, olivine and calcite (Fig. 4c). Clinohumite, brucite, magnetite and apatite are minor; perovskite, baddeleyite,

tazheranite, calcirtite, zirconolite, zirkelite, geikielite and others are accessory. Calcite is medium- to coarse-grained. The mineral shows elevated MgO content (up to 2 wt.%). Olivine forms crystals of variable size (mm to 2 cm) and contains inclusions of calcite, spinel, and accessory minerals. Along the rims, olivine is sometimes altered to calcite serpentine. Olivine is $Fo_{98–100}$. Spinel occurs as octahedral crystals and displays fine-grained intergrowths with olivine. It contains higher TiO_2 (up to 0.7 wt.%) and lower FeO contents (up to 3.7 wt.%) compared to spinel from exoskarns.

Brucite marble

The rock shows a massive texture of uniformly distributed idiomorphic grains of brucite without any signs of ductile deformation and variations of mineral composition. Calcite is the most abundant mineral, forming up to 50–70 % by volume. Sometimes the mineral contains rare dolomite inclusions (Fig. 4d). Calcite has a high MgO content of up to 3.7 wt.%, this is significantly higher than in the calc-silicate rock and endo- and exoskarns; FeO is below the detection limit. Brucite is also a major mineral in the marble, its content ranges between 30 and 50 vol.%. Its composition is $Mg(OH)_2$, sometimes with minor amounts of FeO (up to 0.2 wt.%). The mineral forms onion-skin oval-shaped grains up to 3 mm across (Fig. 4e, f, g). Brucite contains numerous rounded inclusions of calcite, clinohumite, forsterite and apatite (Fig. 4f, g). Rarely, forsterite inclusions are partially replaced by serpentine along microcracks. No relics of periclase have been found in brucite grains. Usually, brucite with onion-skin structure is pseudomorph after hydration of periclase (e.g., Kuleci et al. 2015), although there are some cases without relics of periclase in brucite (e.g., Wenzel et al. 2002; Ganino et al. 2008). Forsterite, clinohumite, magnetite and serpentine are accessory minerals in the rocks. Chemical composition of the brucite marble (Sklyarov et al. 2009) is consistent with the composition of a dolomite marble (Makrygina et al. 1994).

Veinlets parallel-oriented to contacts of brucite marble are composed of calcite and forsterite (Fig. 4h). Clinohumite, brucite and apatite are accessory minerals here. Calcite is medium- to coarse-grained. MgO contents (up to 4 wt.%) are similar to those in calcite from brucite marble. Forsterite is uniformly distributed within veinlets and forms idiomorphic rounded or prismatic grains (Fig. 4h). Along the rims, the mineral is sometimes surrounded by a corona of brucite-calcite and partially replaced by serpentine group minerals (Fig. 4i). The composition of forsterite is close to being ideal (Fo_{100}).

Country dolomite marbles

The dolomite marble is a massive rock, which is composed of medium- to coarse-grained dolomite grains. Tremolite and calcite forms single rare grains (Fig. 4j). Dolomite and calcite contain no measurable impurities.

Stable isotope studies

Carbon and oxygen isotope compositions of carbonate minerals

Oxygen and carbon isotope compositions of calcite from marbles and skarn zones are shown in Table 1, and Figs. 5 and 6. The $\delta^{13}C$ and $\delta^{18}O$ values of country dolomite is 2.4 and 27.5 ‰, accordingly. In contrast, carbon and oxygen isotope compositions of country calcite marble is highly variable. The $\delta^{13}C$ values of calcite from brucite marble and the skarn zone are lower than those of country marble and do not show any significant linear decrease towards the contact with nepheline syenite (Fig. 6). The $\delta^{18}O$ is essentially unchanged within brucite marble, but the $\delta^{18}O$ values are lower within about 50 m of the contact of the marbles as well as the exo-and endoskans (Fig. 6). Notably, the $\delta^{18}O$ values of calcite increase from the proximal to distal zone in vein-like bodies of brucite marbles at contacts with gabbro (Table 1, profile 3).

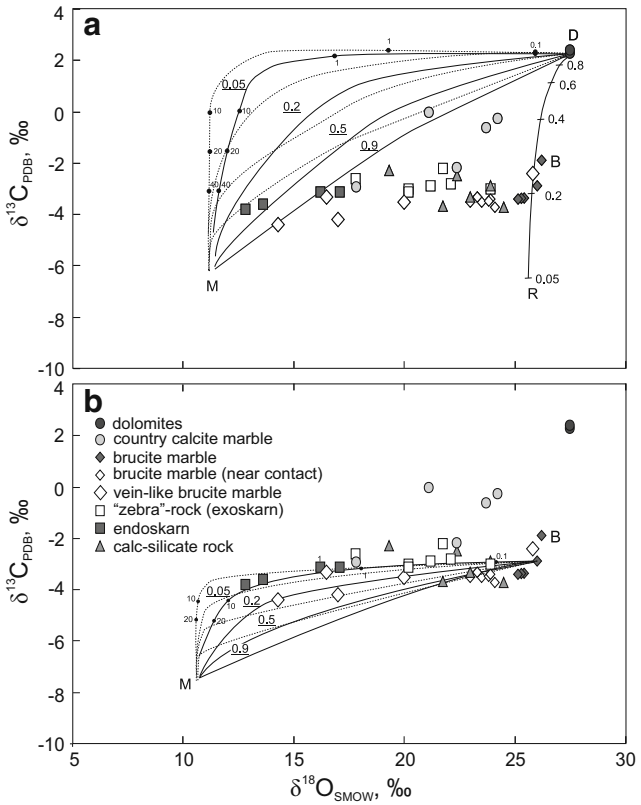

Fig. 5 **a**, **b** Carbon and oxygen isotope diagram for the Tazheran carbonates. The curves of D-M and B-M trends show the effect of fluid-rock interaction for the open (dashed lines) and the closed (solid lines) system, with different X_{CO2} (underlined digits) and atomic oxygen ratios of fluid to rock (dark dotes). Curve D-R is a Rayleigh fractional decarbonation labeled with residual carbon mole fraction

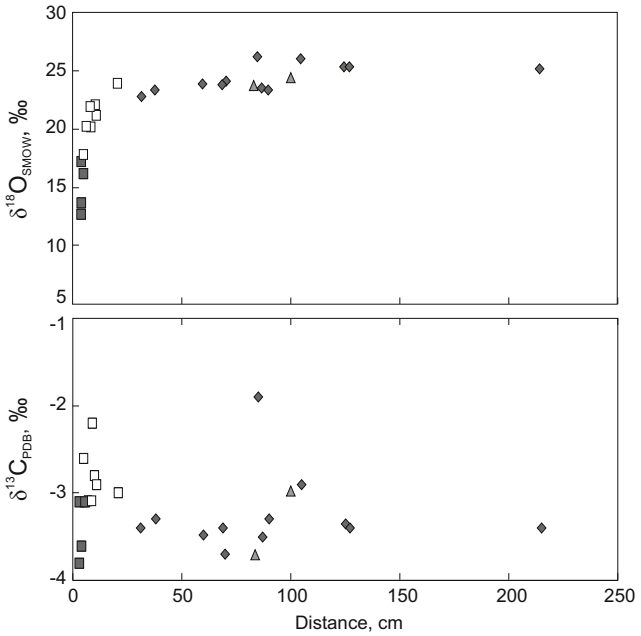

Fig. 6 $\delta^{18}O$ and $\delta^{13}C$ versus distance (centimeters) from the contact of the Tazheran magmatic rocks. Symbols are in Fig. 4

Oxygen and hydrogen isotope compositions of silicates and oxides

Oxygen and hydrogen isotope compositions of minerals from various skarn and magmatic rocks are given in Table 5. The $\delta^{18}O$ values of the minerals from alkaline syenite and nepheline syenite are higher than the average mantle values (about 5.5 ‰), but consistent with the oxygen isotope composition of typical granitic rocks (6–10 ‰, Hoefs 2009). The temperature of nepheline syenite formation was estimated by Konev and Samoylov (1974) at above 770 °C using the feldspar-nepheline geothermometer calibrated by Perchyuk (1965). That temperature was used in calculation of oxygen and hydrogen isotope values of coexisting fluids. The exact temperatures for alkaline syenite formation are unknown. However, magmatic phlogopite would typically be in equilibrium with magmatic waters at temperatures above 800–850 °C. The $\delta^{18}O$ and δD values for estimated fluids in syenite and nepheline syenite are presented in Table 5, Figs. 7 and 8. Their oxygen isotope compositions are slightly enriched compared to the range of magmatic waters (Sheppard 1986).

Table 5 Values of $\delta^{18}O$ and δD for minerals from rocks of skarn zone and country rocks, Tazheran massif

Rock type		Syenite	Nepheline syenite	Endoskarn		Exoskarn		Calc-silicate rocks				Brucite marble			
Sample		T-7	T-3	T-11 g	T-12	T-2	T-11a	Per-4	T-4	T-24	Se700prv	T-1	T-11b	T-25	T-23
$\delta^{18}O$	Rock	9.3	–	–	–	–	–	–	–	–	–	–	–	–	–
(VSMOW)	Bt	8.0	8.88	8.7	8.3	17.6	–	–	–	–	–	–	–	–	–
	Px	–	–	10.6	10.5		–	–	–	15.9	10.6	–	–	–	–
	Nph	–	–	12.7	–	–	–	–	–	–	–	–	–	–	–
	Kfs	–	11	–	–	–	–	–	–	–	–	–	–	–	–
	Ttn	–	7.7	–	–	–	–	–	–	–	–	–	–	–	–
	Zrn	–	8.8	–	–	–	–	–	–	–	–	–	–	–	–
	Ap	–	–	–	7.1	–	15.6	–	–	–	–	–	–	–	–
	Fo	–	–	–	–	16.3	14.2	16.8	18.1	17.7	16.6	–	–	–	–
	Spl	–	–	–	–	14.7	–	14.9	15.7	17	15.1	–	–	–	–
	Prv	–	–	–	–	–	–	13.2	–	–	–	–	–	–	–
	Brc	–	–	–	–	–	–	–	–	–	–	−1.7	1	−1.2	1.4
δD	Bt	−94.4	−81.6	−108.4	−112.9	–	–	–	–	–	–	–	–	–	–
(VSMOW)	Brc	–	–	–	–	–	–	–	–	–	–	−157.7	−160.9	−159.4	−146.4
Calc. T°C		850–900	770	740*	596*	476**	431**	526 **	534**	552 **	612 **	600	600	600	600
$\delta^{18}O$ fluid	Rock	9.5	–	–	–	–	–	–	–	–	–	–	–	–	–
	Cal	–	–	11.8	11.9	19.2	17	19.5	20.8	20.4	17.7	22.22	23.75	22.5	24.4
	Px	–	–	12.6	12.6	–	–	–	–	–	–	–	–	–	–
	Nph	–	–	13.9	–	–	–	–	–	–	–	–	–	–	–
	Fo	–	–	–	–	20.3	18.2	20.8	22.1	21.6	20.4	–	–	–	–
	Bt	10.3	11.28	11.1	10.8	20	–	–	–	–	–	–	–	–	–
	Kfs	–	11	–	–	–	–	–	–	–	–	–	–	–	–
	Ttn	–	10.2	–	–	–	–	–	–	–	–	–	–	–	–
	Zrn	–	11.5	–	–	–	–	–	–	–	–	–	–	–	–
	Brc	–	–	–	–	–	–	–	–	–	–	3.4	6.1	3.9	6.5
δD fluid	Bt	−73.1	−58.1	−83.7	−80.3	–	–	–	–	–	–	–	–	–	–
	Brc	–	–	–	–	–	–	–	–	–	–	−140.7	−143.9	−142.4	−129.4

Temperature was calculated by calcite-diopside* and calcite-forsterite** pairs (Zheng 1993a). Calculated $\delta^{18}O$ and δD composition of fluid is according to mineral-water fractionations of Suzuoki and Epstein 1976; Zheng 1993a, b; 1998; 1999; Zhao and Zheng 2003; Méheut et al. 2010. Bt-biotite, Px – pyroxene, Nph – nepheline, Kfs – potash feldspar, Ttn – titanite, Zrn – zircon, Ap – apatite, Fo –forsterite, Spl – spinel, Prv – perovskite, Brc – brucite, Cal – calcite

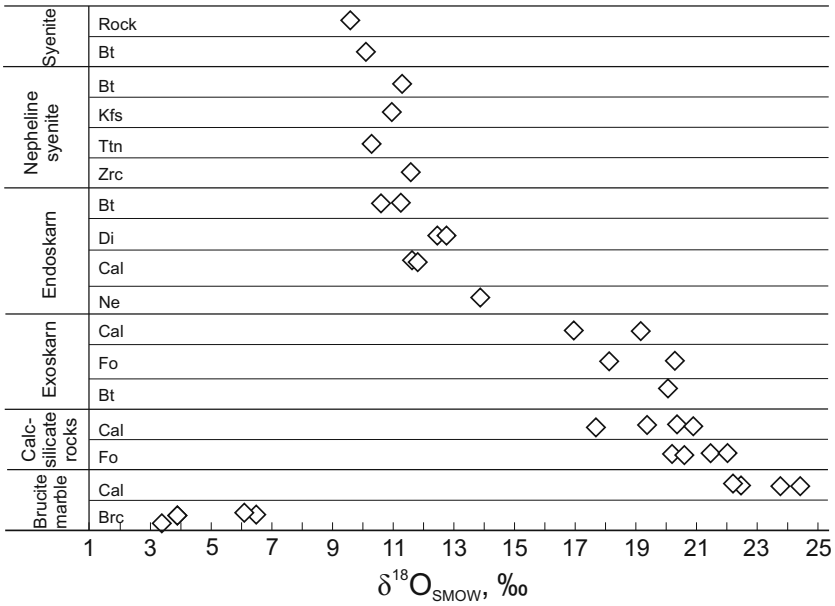

Fig. 7 Calculated $\delta^{18}O$ compositions of fluids in equilibrium with minerals from Tazheran rocks

The $\delta^{18}O$ values of endoskarn minerals range from 7.1 to 12.7 ‰. The δD values in the hydrous minerals from endoskarn are depleted in comparison with minerals from syenite and nepheline syenite implying an influence of skarn-forming fluids. The calcite–diopside isotope fractionation applied in endoskarn samples gave a range of temperatures from 596 to 740 °C. At those temperatures, oxygen isotope composition of coexisting fluids estimated assuming an equilibrium with endoskarn minerals is similar to those of syenites (Table 5, Fig. 7).

Minerals of exoskarn and calc-silicate rocks are characterized by high $\delta^{18}O$ relative to the minerals from magmatic rocks and endoskarn. The apparent temperature of exoskarn equilibration calculated for calcite-forsterite pairs is in the range of 430–476 °C. Calcite-forsterite pairs from the calc-silicate rocks yield slightly higher temperatures (up to 612 °C) compared to exoskarn. Oxygen isotope composition of a coexisting fluid is 17–20 ‰ for the exoskarn and 17.7–22 ‰ for the calc-silicate rocks. Thus, the calculated $\delta^{18}O$ values of the coexisting fluids clearly increase from syenite and nepheline syenite throughout endoskarn to exoskarn and calc-silicate rocks (Fig. 7).

Brucite has low $\delta^{18}O$ (Table 5, Fig. 6). Accepting the temperature of brucite marble formation at around 550 °C (according to the limits of brucite stability, Lentz 1999 and our thermodynamic calculation, see below), the calculated $\delta^{18}O$ for a fluid equilibrated with calcite is 22–24 ‰, and with brucite is 3.5–6.5 ‰. The δD values in brucite are depleted compared to the hydrous minerals from syenite and endoskarn

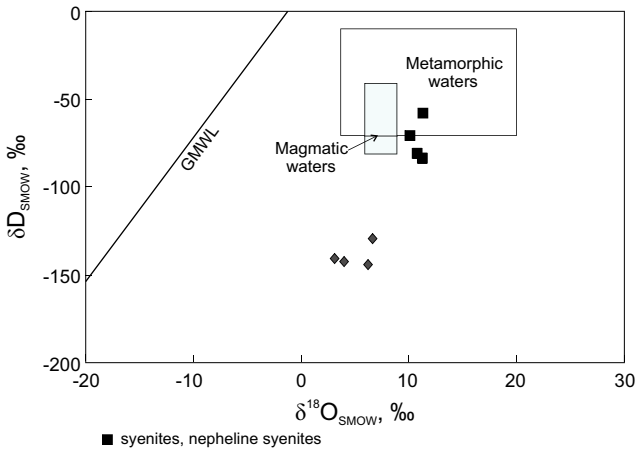

Fig. 8 δD versus $\delta^{18}O$ plot for calculated waters in equilibrium with minerals from Tazheran rocks. Symbols are in Fig. 4. Also shown for reference are: the Global Meteoric Water Line (GMWL) (Craig 1961); magmatic and metamorphic waters (Sheppard 1986)

Table 6 $\delta^{13}C$ and $\delta^{18}O$ depletion of marbles during the volatilization process in open system

Mole fraction of remaining carbon in system	$\delta^{13}C$	$\delta^{18}O$
$\delta^{13}Ci = 2.4$ ‰. $\delta^{18}Oi = 27.5$ ‰		
1	2.40	27.50
0.9	2.17	27.30
0.8	1.91	27.08
0.7	1.62	26.86
0.6	1.28	26.63
0.5	0.88	26.38
0.4	0.39	26.13
0.3	−0.25	25.86
0.2	−1.13	25.57
0.1	−2.65	25.27
0.05	−4.17	25.11
0.01	−7.68	24.95

(Table 5, Fig. 8). Moreover, calculated δD for a fluid equilibrated with brucite is −129 to −144 ‰. Such $\delta^{18}O$ and δD depletion is common in contact aureoles and related to influx of meteoric waters (e.g., Criss and Taylor 1986; Jamtveit and Anderson 1993; Bowman 1998).

Discussion

Isotope depletion in brucite marble

We consider it noteworthy that the brucite marble has lower $\delta^{13}C$ values than country dolomite marble (Fig. 5). The possible explanations for this depletion are: (1) effect of carbon and oxygen removal by decarbonation, and (2) fluid-rock interaction (e.g., Bowman 1998; Baumgartner and Valley 2001).

For calculation of the open system decarbonation we chose the highest $\delta^{18}O$ and $\delta^{13}C$ values for country dolomite marble (27.5 ‰ and 2.4 ‰, accordingly) and a temperature of 550 °C (Lentz 1999 as well as results of our thermodynamic calculations (see section 6.2, average values)). The results are presented in Table 6 and Fig. 5 (the D-R curve). In case all dolomite was consumed during decarbonation with formation of calcite and brucite, the remaining carbon fraction is estimated at ~40-50 %. This agrees well with our petrographic observations and thermodymanic calculations showing that brucite marble contains around 60 % calcite and around 40 % brucite. Thus, in case of complete dolomite consumption, the calculated $\delta^{13}C$ of the residual calcite should be 0.87 ‰, whereas the value for the mineral in brucite marble is lower (−1.9 ‰). It follows that decarbonation is important but insufficient for producing the observed depletion in ^{13}C in brucite marble.

The carbon isotope depletion also can be explained in two ways: (1) by interaction with Tazheran magmatic waters or (2) the involvement of aqueous fluids depleted in C^{13}.

According to the isotope data, brucite marble cannot be a product of fluid-rock interaction during emplacement of Tazheran magmatic rocks. Figure 5a shows the D-M trend of fluid-rock interaction between country dolomite marble (D) and Tazheran magmatic waters (M), evaluated carbon and oxygen isotope compositions for the latter are −5 ‰ (average mantle value) and 10.8 ‰ (the average $\delta^{18}O$ value for the calculated Tazheran coexisting fluids), accordingly. The $\delta^{13}C$ - $\delta^{18}O$ variation curves of D-M trend in the open and closed systems were calculated at 550 °C and at different X_{CO2} conditions and fluid-rock ratios. One can see that carbon and oxygen isotope values for brucite marble (except two values for vein-like brucite marble) do not lie on the D-M trend of fluid-rock interaction (Fig. 5a).

The mechanism of involvement of water fluids depleted in C^{13} seems more acceptable for the negative $\delta^{13}C$ values for carbonates from brucite marble. Such fluids have been usually interpreted as resulting from participation of organic matter carbon that formed either by oxidation of organic matter or participation of methane. Methane may be produced by thermal decomposition of organic-rich shale and coal or, in lesser degree, carbonate (siderite-bearing) rocks during igneous and metamorphic processes (e.g.,McCollom 2003; Fiebig et al. 2004; Svensen et al. 2004, 2007; Aarnes et al. 2011). This is supported by the fact that the processes of regional metamorphism at amphibolite facies conditions, folding and mantle magmatism were widely developed within the Olkhon collision system at ~500 Ma (Fedorovsky et al. 2010). Unfortunately, no fluid inclusions have been found in minerals from brucite marble which could indicate direct involvement of aqueous CH_4 (and heavier hydrocarbons) bearing fluids. It is important to note that graphite-bearing zones are widespread within the Olkhon collision zone (e.g., Martikhaeva et al. 2009; our observations).

The presence of graphite indicates a possibility of contributions of ^{13}C-depleted carbon to the fluid phase. The $\delta^{13}C$ values for graphite from quarzite (−16.9 ‰), gneiss (−17.6 ‰), gneissic granite (−10.3; −17.6 ‰) and calc-silicate rock (−12.4 ‰) of the Olkhon collision zone are low. These values are slightly higher than the average value of −25 ‰ for organic matter, but significantly lighter than for mantle carbon (−6 ‰) and sedimentary carbonates (0 ‰) (e.g., Hoefs 2009). Probably the fluids from different sources were mixed and led to a new $\delta^{13}C$ for the mixture. We used a multicomponent Rayleigh isotope fractionation (Ray 2009) for the explanation of the observed $\delta^{13}C$ values in graphite.

Figure 9 shows the Rayleigh model evolution curves for graphite precipitating from a $CH_4 + CO_2$ fluid. Calculations were performed at the average temperature of 600 °C for the Olkhon collision zone metamorphism (Sklyarov et al. 2009; Fedorovsky et al. 2010) and a rCH_4-CO_2 value of 0.85. Model calculation reveals that the initial carbon isotope composition of the fluid (−15 ‰). This $\delta^{13}C$ value indicates both organic matter and carbonates as the main sources for carbon.

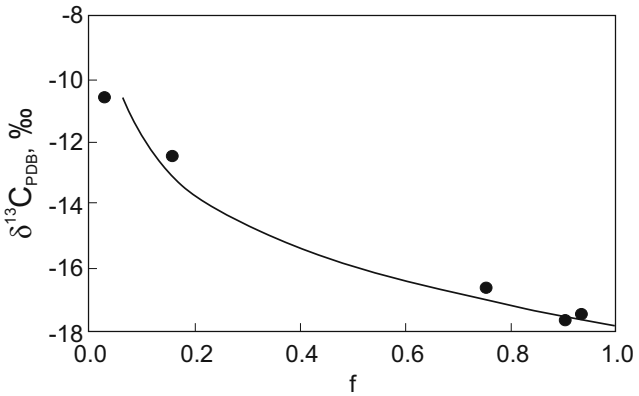

Fig. 9 $\delta^{13}C$ versus *f* (fraction of remaining source) plot for the graphite of the Olkhon collision zone compared with the multicomponent Rayleigh isotope fractionation evolution curve

Thus, we conclude that the stable isotope depletion observed in brucite marble was not due to interaction with fluids realized from Tazheran magmatic rocks (Fig. 5a) and resulted from both decarbonation and direct addition of aqueous fluids depleted in C^{13}. It should be noted that a similar slope of O-C isotope trend and very low values of $\delta^{13}C$ in calcite from the Mottled Zone, Israel, is explained by both volatilization and high temperature exchange of carbonates with bituminous matter (Kolodny and Gross 1974; Baumgartner and Valley 2001).

The numerical thermodynamic modeling of brucite marble genesis

The numerical thermodynamic modeling was carried out in order to determine: (1) the PT-conditions for a formation of the Tazheran brucite marble, (2) the mineral proportion of a possible initial rock (dolomite with admixture of tremolite, clinochlore and quartz), initial rock decarbonation and interaction with CH_4-bearing water (depleted in C^{13}). The simulated system represents a rectangular area in PT-space restricted by 500–800 °C and 500–5000 bars with increments of 25 °C and 500 bars, respectively. Independent components of the system include Mg, Ca, C, H, O. The initial mineral composition of the system includes stoichiometrically pure dolomite $Ca_{0.5}Mg_{0.5}CO_3$, tremolite $Ca_2Mg_5Si_8O_{22}(OH)_2$, clinochlore $Mg_5Al(AlSi_3O_{10})(OH)_8$ and quartz SiO_2. Fluid is represented by an aqueous solution with CH_4. The maximal initial concentration of methane for the lower model conditions (T = 500 °C, P = 500 bars) has been estimated at 0.01428 g/kg H_2O (Ilchenko et al. 1982).

Examination of the model shows that the most appropriate initial composition is dolomite (89 wt.%), tremolite (8 wt.%), and clinochlore (3 wt.%), with excess of water and the complete absence of quartz. The complete flushing of initial rock by CH_4-bearing water under different model conditions led to the equilibrium mineral assemblages that are shown on Fig. 10. Calcite is stable throughout the whole model PT range, with the maximum (~63.34 wt.%) in the range of 600–675 °C and 500–2500 bars, and with the minimum (~46.63 wt.%) in the range of 700–725 °C and 4000–5000 bars (Fig. 10). Calcite and brucite are stable in the range of 500–580 °C and 1000–5000 bars with calcite content of about 50–54 wt.%, whereas the forsterite-brucite-calcite assemblage is stable at slightly higher temperature with the same calcite content (Fig. 10).

The disappearance of dolomite may be explained by several mineral reactions. Dolomite can break down to calcite and periclase followed by hydration of periclase to form brucite:

$$\text{dolomite} = \text{calcite} + \text{periclase} + CO_2,$$
$$\text{periclase} + H_2O = \text{brucite}$$

However, periclase was not observed in the Tazheran brucite marble. This is probably due to the high reactivity of periclase, which tends to form brucite or it was the result of direct decarbonation and hydration via the reaction:

$$\text{dolomite} + H_2O = \text{calcite} + \text{brucite} + CO_2$$

In addition, forsterite –calcite veinlets occur in brucite marble. Forsterite grains are sometimes surrounded by a calcite-brucite corona. It can indicate growth in the course of a calcite-brucite forming reaction such as:

$$\text{tremolite} + 12\text{dolomite} = 14\text{calcite} + 8\text{forsterite} + \text{brucite} + 10CO_2$$

Isotope depletion in rocks of the skarn zone

The emplacement of brucite marble, syenite and gabbro was synchronous according to field observations (see discussion below) and the process was accompanied by the formation of endo- and exoskarns at the contact between syenite and

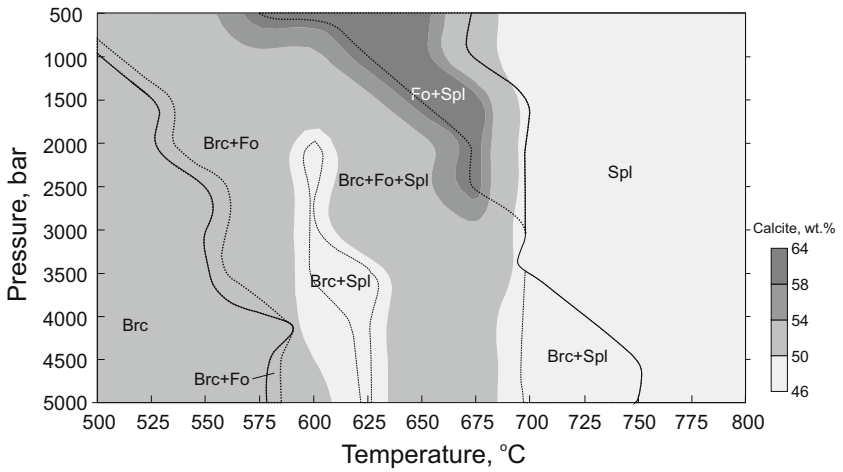

Fig. 10 PT-diagram of the estimated model assemblages

brucite marble. Our isotope data show that the rocks of the skarn zone tend to show systematically lower $\delta^{18}O$ values (Fig. 6). Such linear isotope depletion could be attributed to fluid-rock interaction. The initial $\delta^{18}O$ and $\delta^{13}C$ values in calcite and magmatic fluid are 25.6 ‰ and −3 ‰ (the average $\delta^{18}O$ and $\delta^{13}C$ values for mineral from brucite marbles, far from contact), as 10.3 ‰ and −5 ‰, accordingly for the calculation of final compositions of respective isotopes. The B-M mixing trend was drawn at a temperature of 560 °C according to the calculated temperature for skarn rocks with varying X_{CO2} and fluid-rock ratios in open and closed systems (Fig. 5b). The $\delta^{18}O$ and $\delta^{13}C$ values measured in calcite from skarns, including calc-silicate rocks overlap on the depletion curves of the B-M trend with X_{CO2} up to 0,2.

Thus, brucite marble interacted during the emplacement with magmatic rocks and the process was accompanied by the formation of skarns. The oxygen isotope composition of minerals in the skarn zone is affected by this interaction.

The emplacement of brucite marble: ductile flow or product of melting?

Konev and Samoylov (1974) interpreted the brucite marble as metamorphosed xenoliths of dolomite in syenite. Under influence of the syenite the dolomite marble was transformed to periclase-calcite marbles, later periclase was replaced by brucite as a result of hydration. Such simple explanation strikes with geological and structural controversies discussed in the geological background section. Sklyarov et al. (2009, 2013) discussed possible scenarios of the brucite marble emplacement: (1) injection (protrusion) of dolomite with subsequent transformation of periclase marble to brucite marble; (2) injection (protrusion) of periclase marble with a following replacement of periclase by brucite or injection of brucite marble; (3) intrusion of crustal water-saturated carbonate melt. The first scenario seems unrealistic because it is not supported by our isotope data. In addition, the peak of temperature passed at the time of syenite emplacement and when dolomites were metamorphosed. Ductile flow of periclase marbles (the second scenario) may be possible. Formation of endo- and exoskarns as well as isotope data of skarns confirm this scenario. However, ductile flow of periclase marbles would result in segregation and structuring of "hard" periclase in a "soft" calcite matrix (like in a blastomylonite). For example, banded and lenticular segregations of silicate minerals are widespread in the melange marble zones within the Olkhon collision system (Sklyarov et al. 2013). The ductile flow signatures are absent from the vein-like bodies of brucite marble. They have a massive isotropic texture as well as display bodies of complex shape. Finally, complete preservation of onion-skin oval-shaped brucite grains contradicts the scenario of ductile flow of brucite marbles.

The emplacement of brucite marble in a molten state can also be possible (Sklyarov et al. 2009, 2013), although zebra rocks formed in contact of brucite marble with syenite seems to contradict this scenario. It is suggested that the zebra rocks are the result of post-nucleation geochemical self-organization (e.g., Holness 1997, 2000; Ganino et al. 2008). Nevertheless, these rocks were established in heterogeneous melt-inducing aureole of the Panzhihua intrusion, China (Ganino et al. 2013). Moreover, intrusion of carbonatites is usually accompanied by formation of fenites (rocks enriched in phlogopite, aegirine, amphiboles, alkali feldspar, apatite) at the contacts (e.g., Le Bas 2008; Pirajno et al. 2014). It can be assumed that the emplacement of brucite marble was in partially crystallized (mushy) state. Although the question of zebra rocks formation still remains open.

The cases of natural occurrences of crustal carbonate melt are rare (Lentz 1999; Abart et al. 2001; Wenzel et al. 2002; Morteani et al. 2013; Ganino et al. 2013). This scenario is consistent with geological and structural data for Tazheran, however there are no direct evidences (melt inclusions in minerals) in the rock. In addition, all silicate minerals in brucite marbles and calc-silicate rocks are products of metasomatic and/or metamorphic processes. The latter, however, does not refute the probability of crystallization of brucite marble and calc-silicate rocks form a melt and it is not ruled out that silicate minerals were crystallized from a melt and later were metasomatically transformed during cooling and interaction of carbonate and silicate components. For example, Vuorinen and Skelton (2004) showed that most silicate minerals in a calcite carbonatite dyke from Alnö Island are the product of country silicate rocks assimilation or interaction with pure calcite melt.

Numerous experiments (e.g., Wyllie and Tuttle 1960; Byrnes and Wyllie 1981; Fanelli et al. 1986; Persikov and Bukhtiyarov 2004) show that melting in the MgO-CaO-H_2O-CO_2 system produces periclase-calcite melt rather than pure calcite melt. At fixed fluid composition ($X_{CO2} = 0.05$), the solidus curve for granite is congruent with the melting curve for calcite at water-saturated conditions, and the melting curve for dolomite is positioned 100 °C below (Lentz 1999). It means that dolomite can start melting earlier than in granites. Moreover, Persikov and Bukhtiyarov (2004) showed that heating of dolomite under water fluid pressure of 100 MPa and $T \leq 530$ °C resulted in its decomposition into periclase and calcite, and release of CO_2 followed by calcite melting. The proposed isotope model of dolomite transformation in brucite marble as a result of decarbonation with participation of fluids depleted in C^{13} does not contravene the experiments.

Another important question is whether brucite crystallized directly from a water-rich magnesium carbonate melt or the magnesium phase (periclase or dolomite) converted into brucite during cooling at the presence of a late low δD water (meteoric water). It is difficult to give a definite answer at

the moment. On the one hand, no periclase relicts in brucite were found and brucite contains unaltered inclusions of clinohumite and forsterite. On the other hand, isotope composition of brucite argues for its formation in equilibrium with a low δD fluid, which is significantly different from that in equilibrium with the hydrous minerals of calc-silicate rock and skarns. In addition, the onion shaped brucite nodules typically form at hydration of periclase (e.g., Kuleci et al. 2015).

Conclusions

(1) The Tazheran brucite marble is not the product of interaction with fluids derived from Tazheran magmatic rocks. The brucite marble was formed both by decarbonation and interaction with fluids depleted in C^{13}. Injection of brucite marble or crustal carbonate melt is a possible explanation for formation of Tazheran brucite marble.

(2) Sub-synchronous emplacement of brucite marble, syenite and gabbro was accompanied by fluid-rock interaction between brucite marble and fluids from the Tazheran magmatic rocks resulting in the formation of skarn rocks. Oxygen isotope compositions of minerals in the skarn zone are depleted as the result of this interaction.

(3) According to numerical thermodynamic modeling, calcite-brucite pair is stable in the range of 500–580 °C and 1000–5000 bars with calcite content of the about 50–54 wt.%.

Acknowledgments We would like to thank two anonymous reviewers for their constructive comments on this paper. We are grateful to the editor Christoph Hauzenberger for appreciated suggestions and editorial handling of manuscript. This study was funded by the research RFFI projects 14-05-00180 (isotope studies), 16-05-00202 (geological investigations) and the President of the Russian Federation grant MK-6268.2016.5 (petrographic and mineralogical studies).

References

Aarnes I, Fristad K, Planke S, Svensen H (2011) The impact of host-rock composition on devolatilization of sedimentary rocks during contact metamorphism around mafic sheet intrusions. Geochem Geophy Geosy 12:1–11

Abart R, Schmid R, Harlov D (2001) Metasomatic coronas around hornblendite xenoliths in granulite facies marble, Ivrea Zone, N-Italy I: constraints on component mobility. Contrib Min Petr 141: 473–493

Baumgartner LP, Valley JW (2001) Stable isotope transport and contact metamorphic fluid flow. In: Valley JW, Cole DR (eds) Stable isotope geochemistry. Rev Mineral Geochem, vol 43. Mineral Soc Am, Chantilly, pp 415–467

Bowman JR (1998) Stable-isotope systematics of skarns. In: Lentz DR (ed) Mineralized Intrusion-Related Skarn Systems, vol 26. Mineral Assoc Can, Short Course, Ottawa, pp 99–145

Byrnes AP, Wyllie PJ (1981) Subsolidus and melting relations for the joinCaCO3-MgCO3 at 10 kbar. Geochim Cosmochim Acta 45: 321–328

Chacko T, Mayeda TK, Clayton RN, Goldsmith JR (1991) Oxygen and carbonisotope fractionation between CO_2 and calcite. Geochim Cosmochim Acta 55:2867–2882

Chakrabarty A, Mitchell RH, Ren M, Saha PK, Pal S, Pruseth KL, Sen AK (2016) Magmatic, hydrothermal and subsolidus evolution of the agpaitic nepheline syenites of the Sushina Hill Complex, India: implications for the metamorphism of peralkaline syenites. Miner Mag (in press)

Chudnenko KV (2010) Thermodynamic modeling in geochemistry: the theory, the algorithms, the software, the applications. GEO, Novosibirsk **(In Russian)**

Craig H (1961) Isotope variations in meteoric waters. Science 133:1702–1703

Criss RE, Taylor HP (1986) Meteoric hydrothermal systems. In: Valley JW, Taylor HP Jr, O'Neil JR (eds) Stable isotopes´in high temperature geological processes. Rev Mineral vol 16. Mineral Soc Am, Chantilly, pp 373–424

Deer WA, Howie RA, Zussman J (1997) Rock-forming minerals series. The Geological Society Publishing House, Bath

Dobretsov NL, Buslov MM (2007) Late Cambrian-Ordovician tectonics and geodynamics of Central Asia. Russ Geol Geophys 48(1):71–82

Donskaya TV, Gladkochub DP, Fedorovsky VS, Sklyarov EV, Cho M, Sergeev SA, Demonterova EI, Mazukabzov AM, Lepekhina EN, Cheong W, Kim J (in press) Pre-collisional (>0.5 Ga) complexes of the Olkhon Terrane (Southern Siberia) as an Echo of Events in the Central-Asian Orogen. Gondwana Res

Fanelli MT, Cava N, Wyllie PJ (1986) Calcite and dolomite without portlandite at a new eutectic in CaO–MgO–CO_2–H_2O with applications to carbonatites. Bulg Ac Sci, Sofia, pp 313–322

Fedorovsky VS (2004) Geological map of the south-western part of Olkhon region: 1:100000 scale. GGM RAS, Moscow **(in Russian)**

Fedorovsky VS, Vladimirov AG, Khain EV, Kargopolov SA, Gibsher AS, Izokh AE (1995) Tectonics, metamorphism and magmatizm in collision zones of central Asian caledonides. Geotectonics 3:3–22

Fedorovsky VS, Sklyarov EV, Mazukabzov AM, Kotov AB, Lavrenchuk AV, Starikova AE (2009) Geological map of Tazheran massif: 1: 100000 scale, Moscow, A1 TIS (in Russian)

Fedorovsky VS, Sklyarov EV, Izokh AE, Kotov AB, Lavrenchuk AV, Mazukabzov AM (2010) Strike-slip tectonics and subalkaline mafic magmatism in the Early Paleozoic collisional system of the western Baikal region. Russ Geol Geophys 51:534–547

Fiebig J, Chiodini G, Caliro S, Rizzo A, Spangenberg J, Hunziker JS (2004) Chemical and isotopic equilibrium between CO_2 and CH_4 in fumarolic gas discharges: Generation of CH_4 in arc magmatic-hydrothermal systems. Geochim Cosmochim Acta 68:2321–2334

Gallien F, Abart R, Wyhlidal S (2007) Contact metamorphism and selective metasomatism of the layered Bellerophon Formation in the eastern Monzoni contact aureole, northern Italy. Miner Petrol 91: 25–53

Ganino C, Arndt NT, Zhou M-F, Gaillard F, Chauvel C (2008) Interaction of magma with sedimentary wall rock and magnetite ore genesis in the Panzhihua mafic intrusion, SW China. Miner Deposita 43:677–694

Ganino C, Arndt NT, Chauvel C, Jean A, Athurion C (2013) Melting of carbonate wall rocks and formation of the heterogeneous aureole at the margins of the Panzhihua intrusion, China. Geosci Front 4:535–546

Gladkochub DP, Donskaya TV, Fedorovskii VS, Mazukabzov AM, Sklyarov EV, Lavrenchuk AV, Lepekhina EN (2014) Fragment of the Early Paleozoic (similar to 500 Ma) island arc in the structure of the Olkhon Terrane, Central Asian fold belt. Dokl Earth Sci 457: 905–909

Hoefs J (2009) Stable isotope geochemistry. Springer, Berlin, p 200

Holness MB (1997) Geochemical self-organization of olivine-grade contact metamorphosed chert nodules in dolomite marble, Kilchrist, Skye. J Metamorph Geol 15:765–775

Holness MB (2000) Metasomatism and self-organization of dolerite dike-marble contacts: Beinn an Dubhaich, Skye. J Metamorph Geol 18: 103–118

Horita J (2001) Carbon isotope exchange in the system CO_2-CH_4 at elevated temperatures. Geochim Cosmochim Ac 65:1907–1919

Ilchenko VP, Bochkaryov AV, Subbota MI (1982) Organic water and its role in the formation of oil-gas-hydro-chemical anomalies. Geol Oil Gas 7:57–59 **(In Russian)**

Ireland TR, Compston W, Williams IS, Wendt I (1990) U–Th–Pb systematics of individual perovskite grains from the Allende and Murchison carbonaceous chondrites. Earth Planet Sci Lett 101: 379–387

Jamtveit B, Anderson T (1993) Contact metamorphism of layered shale-carbonate sequences in the Oslo Rift. 3. The nature of skarn-forming fluids. Econ Geol 88:1830–1849

Johnson JW, Oelkers EH, Helgeson HC (1992) SUPCRT92: A software package for calculating the standard thermodynamic properties of minerals, gases, aqueous species, and reactions from 1 to 5000 bars and 0 °C to 1000 °C. Comput Geosci 18(7):899–947

Karpov IK, Chudnenko KV, Kulik DA (1997) Modeling chemical mass transfer in geochemical processes: thermodynamic relations, conditions of equilibria, and numerical algorithms. Am J Sci 297(8):767–806

Kinni PD, Griffin BJ, Kheamen LM, Brakhfogel FF, Spetsius ZV (1997) Determination of U-Pb age of perovskites from Yakutian kimberlites by ion-ion mass-spectrometer (SHRIMP) method. Russ Geol Geophys 38(1):91–99

Kolodny Y, Gross S (1974) Thermal metamorphism by combustion of organic matter: isotope and petrologic evidence. J Geol 82:489–506

Konev AA, Samoylov VS (1974) Contact metamorphism and metasomatism in aureole of Tazheran massif, Novosibirsk, Nauka 246 (in Russian)

Konev AA, Grudinin MI, Ostapenko YP (1967) Tazheran massif of alkaline gabbro, Olkhon region. R Geol Geophys 77:120–122

Konev AA, Ushchapovskaya ZF, Kashaev AA, Lebedeva VS (1969) Tazheranite, a new calcium-titanium-zirconium mineral. Dokl Akad Nauk SSSR 186:917–920

Konev AA, Lesedeva VS, Kashaev AA, Ushchapovskaya ZF (1970) Azoproite, a new mineral of the ludwigite group. Za Vses Min Ova 99(2):225–231 **(in Russian)**

Kuleci H, Schmidt C, Rybacki E, Petrishcheva E, Abart R (2015) Hydration of periclase at 350 °C to 620 °C and 200 MPa: Experimental calibration of reaction rate. Miner Petrol 110:1–10

Le Bas MJ (2008) Fenites associated with carbonatites. Can Miner 46: 915–932

Lentz DR (1999) Carbonatite genesis: A reexamination of the role of intrusion-related pneumatolytic skarn processes in limestone melting. Geology 27:335–338

Li Q, Li X, Liu Y, Wu F, Yang J, Mitchell RH (2010) Precise U–Pb and Th–Pb age determination of kimberlitic perovskites by secondary ion mass spectrometry. Chem Geol 269:396–405

Makrygina VA, Petrova ZI, Konev AA (1994) Geochemistry metacarbonate rocks Priol'honya and Ol'khon Island (Western Baikal region). Geochem Int 10:1437–1450

Martikhaeva DK, Makrygina VA, Polozov AG (2009) Composition of carbon-bearing compounds in marbles from the Tunka, Eastern Sayan, and Ol'khon metamorphic complexes. Geochem Int 7:736–740

McCollom TM (2003) Formation of meteorite hydrocarbons from thermal decomposition of siderite ($FeCO_3$). Geochim Cosmochim Acta 67:311–317

Méheut M, Lazzeri M, Balan E, Mauri F (2010) First-principles calculation of H/D isotope fractionation between hydrous minerals and water. Geochim Cosmochim Acta 74:3874–3882

Morteani G, Kostitsyn YA, Gilg HA, Preinfalk C, Razakamanana T (2013) Geochemistry of phlogopite, diopside, calcite, anhydrite and apatite pegmatites and syenites of southern Madagascar: evidence for crustal silicocarbonatitic (CSC) melt formation in a Panafrican collisional tectonic setting. Int J Earth Sci 102(3):627–645

Perchyuk LL (1965) Paragenesis of nepheline with alkali feldspar as indicator of thermodynamic conditions of mineral equilibrium. Dokl Akad Nauk 161(4):932–935

Persikov ES, Bukhtiyarov PG (2004) Experimental study of the mechanisms of calcite and dolomite melting at high fluid pressures. Electronic Scientific Information Journal "Herald of the Department of Earth Sciences RAS" no. 1(22). Available online: http://geo.web.ru/conf/khitariada/1-2004/informbul-1_2004/term-13e.pdf

Pirajno F, González-Álvarez I, Chen W, Simonetti A, Kyser K, le Grass M (2014) The Gifford Creek ferrocarbonatite complex, Gascoyne Province, Western Australia: associated fenitic alteration and a putative link with the ~1075 Ma Warakurna LIP. Lithos 202:100–119

Povoden E, Horacek M, Abart R (2002) Contact metamorphism of siliceous dolomite and impure limestones from the Werfen formation in the eastern Monzoni contact aureole. Miner Petrol 76:99–120

Ray JS (2009) Carbon isotope variations in fluid-deposited graphite: evidence for multicomponent Rayleigh isotope fractionation. Int Geol Rev 51(1):45–57

Scheele N, Hoefs J (1992) Carbon isotope fractionation between calcite, graphite, and CO_2: an experimental study. Contrib Mineral Petr 112: 35–45

Sharp ZD (1990) A laser-based microanalytical method for the in situ determination of oxygen isotope ratios of silicates and oxides. Geochim Cosmochim Acta 54:1353–1357

Sharp ZD, Atudorei V, Durakiewicz T (2001) A rapid method for determination of hydrogen and oxygen isotope ratios from water and hydrous minerals. Chem Geol 178:197–210

Sheppard SMF (1986) Characterization and isotope variations in natural waters. In: Valley JW, Taylor HP, O'Neil JR (eds) Stable isotopes in high temperature geological processes. Rev Mineral Geochem, vol 16. Mineral Soc Am, Chantilly, pp 165–183

Sklyarov EV, Fedorovsky VS, Kotov AB, Lavrenchuk AV, Mazukabzov AM, Levitsky VI, Sal'nikova EB, Starikova AE, Yakovleva SZ, Anisimova IV, Fedoseenko AM (2009) Carbonatites in collisional settings and pseudo-carbonatites of the Early Paleozoic Ol'khon collisional system. Russ Geol Geophys 50(12):1091–1106

Sklyarov EV, Fedorovsky VS, Kotov AB, Lavrenchuk AV, Mazukabzov AM, Starikova AE (2013) Carbonate and Silicate–Carbonate Injection Complexes in Collision Systems: the West Baikal Region as an Example. Geotectonics 47(3):180–197

SLOP98 (SUPCRT92 data updates). URL: http://geopig.asu.edu/sites/default/files/slop98.dat

Starikova AE, Sklyarov EV, Kotov AB, Sal'nikova EB, Fedorovskii VS, Lavrenchuk AV, Mazukabzov AM (2014) Vein calciphyre and contact Mg skarn from the Tazheran massif (Western Baikal area, Russia): Age and genesis. Dokl Earth Sci 457(2):1003–1007

Suzuoki T, Epstein S (1976) Hydrogen isotope fractionation between OH-bearing minerals and water. Geochim Cosmochim Acta 40: 1229–1240

Svensen H, Planke S, Malthe-Sørenssen A, Jamtveit B, Myklebust R, Eidem T, Rey SS (2004) Release of methane from a volcanic basin as a mechanism for initial Eocene global warming. Nature 429:542–545

Svensen H, Planke S, Chevallier L, Malthe-Sørenssen A, Corfu B, Jamtveit B (2007) Hydrothermal venting of greenhouse gases

triggering Early Jurassic global warming. Earth Planet Sci Lett 256: 554–566

Taylor HPJ (1977) Water/rock interaction and the origin of H2O in granitic batholiths. J Geol Soc Lon 133:509–558

Valley JW (1986) Stable isotope geochemistry of metamorphic rocks. In: Valley JW, Taylor HP, O'Neil JR (eds) Stable isotopes in high temperature geological processes. Rev Mineral Geochem, vol 16. Mineral Soc Am, Chantilly, pp 445–490

Vasiliev VI, Damdinov BB (2013) The physical-chemical model of Eastern Sayan ore-bearing rodingites and magnetite-chlorite-epidotic metasomatites. Lithosph 5:72–96 **(in Russian)**

Vasiliev VI, Chudnenko KV, Zhatnuev NS, Vasilieva EV (2009) The computer modeling of geological objects by the example of subduction zone profile. Geoinformatica 3:15–30 **(in Russian)**

Vuorinen JH, Skelton ADL (2004) Origin of silicate minerals in carbonatites from Alno Island, Sweden: magmatic crystallization or wall rock assimilation. Terra Nov. 16:210–215

Wenzel T, Baumgartner LP, Brugmann GE, Konnikov EG, Kislov EV (2002) Partial melting and assimilation of dolomitic xenoliths by mafic magma: the Ioko-Dovyren Intrusion (North Baikal region, Russia). J Petrol 43:2049–2074

Wyllie PJ, Tuttle OF (1960) The system $CaO-CO_2-H_2O$ and the origin of carbonatites. J Petrol 1:1–46

Yang YH, Wu FY, Wilde SA, Liu XM, Zhang YB, Xie LW, Yang JH (2009) In situ perovskite Sr–Nd–Hf isotope constraints on the petrogenesis of the Ordovician Mengyin Kimberlites in the North China Craton. Chem Geol 264:24–42

Zhao ZF, Zheng YF (2003) Calculation of oxygen isotope fractionation in magmatic rocks. Chem Geol 193:59–80

Zheng Y-F (1993a) Calculation of oxygen isotope fractionation in anhydrous silicate minerals. Geochim Cosmochim Acta 57:1079–1091

Zheng Y-F (1993b) Calculation of oxygen isotope fractionation in hydroxyl-bearing silicates. Earth Planet Sci Lett 120:247–263

Zheng Y-F (1998) Oxygen isotope fractionation between hydroxide minerals and water. Phys Chem Miner 25:213–221

Zheng Y-F (1999) Oxygen isotope fractionation in carbonate and sulfate minerals. Geochem J 33:109–126